Journal of Colloid and Interface Science 336 (2009) 273–284

Contents lists available at ScienceDirect

Journal of Colloid and Interface Science

www.elsevier.com/locate/jcis

Effect of disjoining pressure on the drainage and relaxation dynamics of liquid films with mobile interfaces

Sonia S. Tabakova [a,c], Krassimir D. Danov [b,*]

[a] Laboratory of Physicochemical Hydrodynamics, Institute of Mechanics, Bulgarian Academy of Science, 1113 Sofia, Bulgaria
[b] Laboratory of Chemical Physics and Engineering, Faculty of Chemistry, University of Sofia, 1164 Sofia, Bulgaria
[c] Department of Mechanics, TU-Sofia, Branch Plovdiv, 4000 Plovdiv, Bulgaria

ARTICLE INFO

Article history:
Received 4 December 2008
Accepted 14 March 2009
Available online 8 April 2009

Keywords:
Dynamics and relaxation of thin liquid films
Tangentially mobile surfaces
Disjoining pressure effects
Arbitrary values of the Reynolds number
Generalized lubrication approximation
Stability and rupture of thin liquid films

ABSTRACT

This work presents a generalized lubrication approximation of the drainage and relaxation of thin liquid films with tangentially mobile surfaces. The proposed model accounts for the dynamic effects and the role of surface forces of intermolecular origin. The van der Waals and hydrophobic attractive and the electrostatic and steric repulsive components of the disjoining pressure are included in the numerical calculations of the dynamics and relaxation of one-dimensional films. Different regimes of film drainage are discussed: regular and unstable mechanisms of thinning depending on the magnitude of the Reynolds number; pimple formation in the presence of large enough attractive surface forces; and stabilizing effects of the disjoining pressure repulsive components. In the case of relaxation, it is proven that the disturbances in the film thickness: decrease exponentially to the equilibrium state without taking into account the role of the disjoining pressure; increase very fast to the point of film rupture in the presence of attractive surface forces; oscillate with exponentially decreasing amplitudes towards the state of stable equilibrium when the electrostatic and steric repulsive forces are significant.

1. Introduction

The modeling of thin liquid film drainage and stability plays an important role for the thorough comprehension of the emulsion and foam formation and stability under dynamic and static conditions [1–4]. Depending on the magnitude of hydrodynamic forces [2–5], the collision of two emulsion droplets or foam bubbles may be accompanied by deformation, more specifically flattening in the zone of contact and subsequent dimple formation. At close distances between interfaces surface forces of intermolecular origin (namely the disjoining pressure [6]) become active and determine the final stage of film formation. When the attractive components of the disjoining pressure are predominant, the film is unstable and ruptures; if the repulsive forces prevail, an equilibrium thin film is formed between the colliding fluid particles. In addition the fluid phases usually contain different kinds of surface active components: surfactants, protein isolates, polymers, etc. [7]. Surfactants not only influence in different ways the magnitude of the surface forces, but also create gradients of the interfacial tension (Marangoni effect) and give rise to surface dilatational and shear viscosities. The interfacial rheology hinders the mobility of interfaces and reduces the rate of their approach.

The problem of near-contact motion of drops was solved numerically using the Stokes equations written for the bulk phases and taking into account the interfacial rheology of insoluble surfactant monolayers [8,9]. The effect of the van der Waals attraction and the electrostatic repulsion components of the disjoining pressure on the drainage and rupture of a film between drops was studied by Chesters et al. [9] and Blawzdziewicz et al. [10]. These models are too complex for systematic investigation of the different factors affecting the behavior of emulsion systems: they are not applicable for films formed in frames; they are only valid when the inertia terms in the momentum balance equations are negligible, as the Reynolds number is formally substituted by zero. Other simpler models are based on the lubrication approximation [5,7,11,12] when the local film thickness is assumed to be much smaller than the lateral dimensions. These models are developed for different kinds of surfactants (ionic and nonionic), different regimes of adsorption (diffusion or barrier controlled), and different types of interfacial rheology [5,13–18]. The linear and nonlinear stability analysis and the role of intermolecular forces on the critical film thickness are widely studied in the literature; see the review article by Valkovska et al. [19]. However, the lubrication approximation fails for foam surfactant-free films or for films with fully mobile surfaces. Indeed, in lubrication approximation the solution of the hydrodynamic problem is expressed in terms of three unknown functions: the lateral velocity components, w_α ($\alpha = 1, 2$), and the dynamic pressure, q, see Eqs. (2.7) and (2.8) be-

* Corresponding author. Fax: +359 2 962 5643.
E-mail address: KD@LCPE.Uni-Sofia.Bg (K.D. Danov).

0021-9797/$ - see front matter © 2009 Elsevier Inc. All rights reserved.
doi:10.1016/j.jcis.2009.03.084

low. The kinematic boundary condition at the film surface, see Eq. (2.10) below, introduces an additional function, the local film thickness, h. Hence, the kinematic boundary condition does not decrease the number of unknown parameters. To determine them, the dynamic boundary condition at the interface must be taken into account. In lubrication approximation the normal stress boundary condition relates w_α ($\alpha = 1, 2$), q, and h, see Eq. (2.12) below. However, the tangential stress boundary condition, Eq. (A.9), is automatically fulfilled by the leading order solution of the problem. For that reason, the second order terms should be considered. This approach is known in the literature as "the extended lubrication approach" [20–24].

For some recent practical applications it is very important to produce thin liquid films from surfactant-free phases or from phases with a very small amount of surface active components. Similar problems arise when the films are stabilized by nanometer-sized particles. In these cases: (i) the lateral dimensions are much larger than the local film thickness; (ii) the film drainage occurs in a dynamic regime at arbitrary values of the Reynolds number. Modeling of the dynamics of such systems is possible using the extended lubrication approach [20–24], formerly applied to study linear and nonlinear stability of films. This approach has also proved its wide applicability for modeling the drainage and stability of evaporating films [25–30] and for modeling the solidification of free thin films attached to a frame and pulled from a melt [31]. Originally these models account for the van der Waals interactions between interfaces. Recent experimental and theoretical investigations manifest the importance of a number of other components of the disjoining pressure. Experimental measurements show that, even in pure liquid, the gas bubbles have ζ-potential of -65 mV [32], which for the xylene, dodecane, hexadecane, and perfluoromethyldecalin droplets changes from -100 mV to -20 mV, depending on the electrolyte concentration and pH of the solution [33]. The charge accumulation on the surfaces is due to the spontaneous adsorption of hydroxyl ions, which causes electrostatic repulsion between the film interfaces. Many experiments with emulsion and foam films [34–38] suggest that the long range hydrophobic attraction forces can be considerably larger than the van der Waals interactions, and must be included as a disjoining pressure component. At close distances between film interfaces strong steric interactions between adsorbed particles can stabilize film drainage and prevent film rupture [39–41]. The aim of the present study is to take into account the role of different types of intermolecular interactions for the film drainage and stability in dynamic conditions, using the extended lubrication approach.

The paper is organized as follows. In Section 2, we describe the extended lubrication approach applied for films with tangentially mobile surfaces in the framework of the disjoining pressure approach. The dimensionless numbers appearing in the model equations for one-dimensional symmetric films are introduced in Section 3. They take into account the contribution of inertia, interfacial tension, van der Waals, hydrophobic, electrostatic and steric forces. Therein, the boundary conditions and possible regimes of the film drainage and relaxation are discussed. The effect of the intermolecular forces and the magnitudes of the Reynolds and Weber numbers on film drainage are studied in Section 4 and their influence on film relaxation – in Section 5. The general conclusions are given in Section 6.

2. Modeling of the dynamics of thin liquid free films

2.1. Conservation of mass and momentum in the bulk phase

We consider a symmetric thin foam film with a local thickness H (Fig. 1). The bulk phase in the film is described as an incompressible homogeneous liquid with velocity vector **U**, pressure P, constant dynamic viscosity η and density ρ. The Cartesian coordinate system, $OX_1X_2X_3$, is placed in the plane of film symmetry $X_3 = 0$, where X_α ($\alpha = 1, 2$) are the lateral coordinates and X_3 is the vertical coordinate (Fig. 1). The characteristic lateral velocity is U, the lateral length scale is a, and the natural scale of time, T, is a/U. The film thickness, H, is measured with the vertical length scale, b, and is assumed to be so small that the ratio, $\varepsilon \equiv b/a \ll 1$, can be considered as a small parameter in the problem. The dimensionless time, t, the lateral coordinates and components of the velocity vector, x_α and u_α ($\alpha = 1, 2$), are defined as follows

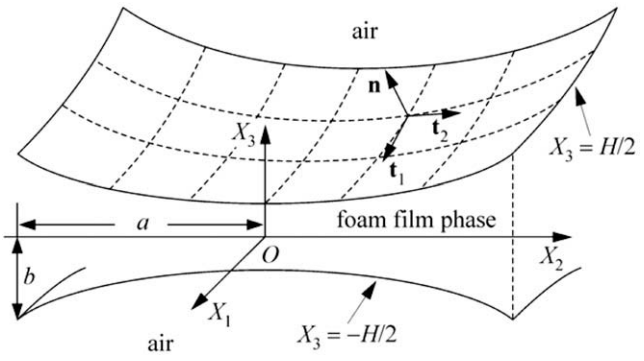

Fig. 1. Sketch of a symmetric thin liquid film with a local film thickness H. The vertical coordinate axis of the Cartesian coordinate system, $OX_1X_2X_3$, is perpendicular to the film middle plane, $X_3 = 0$. The characteristic lateral length, a, is much larger than the characteristic vertical length, b. The position of the upper film surface is defined as $X_3 = H/2$ and the position of the lower one – as $X_3 = -H/2$. The upper surface normal and tangent vectors are **n**, $\mathbf{t}_1$, and $\mathbf{t}_2$, respectively.

$$t \equiv \frac{UT}{a}, \quad x_\alpha \equiv \frac{X_\alpha}{a}, \quad \text{and} \quad u_\alpha \equiv \frac{U_\alpha}{U} \quad (\alpha = 1, 2). \tag{2.1}$$

The dimensionless film thickness, h, the vertical coordinate, x_3, and the vertical component of the velocity, u_3, are introduced through the following relationships

$$h \equiv \frac{H}{b}, \quad x_3 \equiv \frac{X_3}{b}, \quad \text{and} \quad u_3 \equiv \frac{aU_3}{bU}. \tag{2.2}$$

Eq. (2.2) accounts for the facts that: (i) in the case of thin liquid films the vertical component of the velocity is much smaller than the respective lateral components; (ii) the continuity equation must be invariantly expressed in terms of dimensionless quantities [22,24]:

$$\frac{\partial u_\beta}{\partial x_\beta} + \frac{\partial u_3}{\partial x_3} = 0, \quad (\beta = 1, 2). \tag{2.3}$$

In Eq. (2.3) and below we will use the Einstein summation convention, where the Greek letter subscripts (α and β) indicate sums related to the lateral components denoted with indexes 1 and 2.

For Newtonian fluids the momentum balance is described by the Navier–Stokes equation. For foam films with fully mobile surfaces (see Section 2.2) a viscous scale, $\eta U/a$, is appropriate for measuring the pressure P. The dimensionless pressure, p, and the Reynolds number, Re, are introduced by the definitions

$$p \equiv \frac{aP}{\eta U} \quad \text{and} \quad \mathrm{Re} \equiv \frac{\rho a U}{\eta}. \tag{2.4}$$

Using the above expressions, Eqs. (2.1), (2.2) and (2.4), we obtain the dimensionless form of the momentum balance equation in the lateral directions (α, $\beta = 1, 2$) [42]:

$$\mathrm{Re}\left[\frac{\partial u_\alpha}{\partial t} + \frac{\partial}{\partial x_\beta}(u_\beta u_\alpha) + \frac{\partial}{\partial x_3}(u_3 u_\alpha)\right] = -\frac{\partial p}{\partial x_\alpha} + \frac{\partial^2 u_\alpha}{\partial x_\beta \partial x_\beta} + \frac{1}{\varepsilon^2}\frac{\partial^2 u_\alpha}{\partial x_3^2}. \tag{2.5}$$

The respective dimensionless form of the vertical projection of the Navier–Stokes equation reads [42]

$$\mathrm{Re}\left[\frac{\partial u_3}{\partial t}+\frac{\partial}{\partial x_\beta}(u_\beta u_3)+\frac{\partial}{\partial x_3}(u_3 u_3)\right] = -\frac{1}{\varepsilon^2}\frac{\partial p}{\partial x_3}+\frac{\partial^2 u_3}{\partial x_\beta \partial x_\beta}+\frac{1}{\varepsilon^2}\frac{\partial^2 u_3}{\partial x_3^2}. \quad (2.6)$$

The Reynolds number, Re, appearing in Eqs. (2.5) and (2.6) and defined by Eq. (2.4), is assumed not to be very large, i.e. $\mathrm{Re} \leqslant O(1/\varepsilon)$. For example, for water films ($\rho = 10^3$ kg/m^3, $\eta = 10^{-3}$ Pa s) with an initial thickness $b = 1$ mm and a frame lateral length $a = 1$ cm ($\varepsilon = b/a = 0.1$), the lateral velocity, U, at which $\varepsilon\mathrm{Re} = \rho b U/\eta = 1$ is equal to 1 mm/s, thus in that case the model would be applicable for suction velocities smaller than 1 mm/s. The effect of the inertia on the film drainage is discussed in Section 4.1 (see Fig. 3).

Because of the symmetry of the considered problem $\partial u_\alpha/\partial x_3 = 0$ at the middle plane $x_3 = 0$. Taking into account Eq. (2.3) one obtains the leading order solution of Eqs. (2.5) and (2.6) [22]:

$$u_\alpha = w_\alpha(t, x_1, x_2) + O(\varepsilon^2) \quad \text{and}$$

$$p + \frac{\partial w_\beta}{\partial x_\beta} = q(t, x_1, x_2) + O(\varepsilon^2), \quad (2.7)$$

where the functions q and w_α depend on time, t, and lateral coordinates, x_1 and x_2. After substituting Eq. (2.7) into the continuity equation, Eq. (2.3), integrating the obtained result with respect to x_3 and using the symmetry condition $u_3 = 0$ at the middle plane, we obtain the leading order expression for the vertical velocity component:

$$u_3 = -\frac{\partial u_\beta}{\partial x_\beta}x_3 + O(\varepsilon^2). \quad (2.8)$$

The unknown functions h, q, and w_α are determined from the kinematic and dynamic boundary conditions at the film interface $x_3 = h/2$ using an appropriate asymptotic procedure (see Section 2.2 and Appendix A).

2.2. Kinematic and dynamic boundary conditions at the interface

Using the above definitions, Eqs. (2.1) and (2.2), one presents the kinematic boundary condition at the film surface in a simple dimensionless form [42]

$$\frac{\partial h}{\partial t} + u_\beta \frac{\partial h}{\partial x_\beta} = 2u_3 \quad \text{at } x_3 = \frac{h}{2}. \quad (2.9)$$

Through substituting the leading order solutions, Eqs. (2.7) and (2.8), into Eq. (2.9) we obtain the respective expression describing the conservation of mass in the continuous film phase

$$\frac{\partial h}{\partial t} + \frac{\partial}{\partial x_\beta}(h w_\beta) = 0. \quad (2.10)$$

In surfactant-free films the interfacial tension, σ, is constant and the surface shear and dilatational viscosities are negligible. Therefore, in this case, the bulk viscous friction force at the film surface is zero [7]. The leading order of the tangential stress boundary condition at $x_3 = h/2$ is calculated in Appendix A, see Eq. (A.8). After combining the obtained result with the integrated form of Eq. (2.5) in Appendix A, we derive the asymptotic form of the momentum balance equation in the film:

$$\mathrm{Re}\left[\frac{\partial}{\partial t}(h w_\alpha) + \frac{\partial}{\partial x_\beta}(h w_\beta w_\alpha)\right] = -h\frac{\partial}{\partial x_\alpha}\left(q + \frac{\partial w_\beta}{\partial x_\beta}\right) + \frac{\partial}{\partial x_\beta}\left[h\left(\frac{\partial w_\beta}{\partial x_\alpha} + \frac{\partial w_\alpha}{\partial x_\beta} + 2\frac{\partial w_\gamma}{\partial x_\gamma}\delta_{\alpha\beta}\right)\right], \quad (2.11)$$

where $\delta_{\alpha\beta}$ is the Kronecker delta.

It is important to clearly indicate for which systems the momentum balance Eq. (2.11), originally derived for pure liquids, is applicable.

(i) If the solution contains only indifferent electrolytes (salts), then the change of the surface tension with the ionic strength is small, the Gibbs elasticity is small and the Marangoni stress can be neglected [43]. The electrostatic and van der Waals components of the disjoining pressure appear at small film thickness and control the film drainage and stability.

(ii) In the case of small amount of low molecular weight surfactants, the surfactant relaxation time is comparable to the characteristic time of film drainage and the Marangoni effect becomes evident. This effect suppresses the surface mobility and decreases the rate of film thinning [5,13,18]. The account of the Marangoni stress makes the respective analogue of Eq. (2.11) much more complex.

(iii) In the case of large amount of low molecular weight surfactants (close or above the critical micelle concentration) the surfactant relaxation time decreases considerably and it is of the order of or smaller than several microseconds [44]. In these systems the surface tension does not change due to the film drainage and the Marangoni stress can be neglected. From the literature it is known that low molecular weight surfactants have very small values of surface viscosity [45,46] and therefore, the role of interfacial rheology is also negligible. For such systems Eq. (2.11) is valid. In addition to the classical components of the disjoining pressure, the steric, oscillatory, etc. non-DLVO surface forces should be considered.

(iv) Films stabilized by proteins or polymers have significant values of the surface dilatational and shear viscosities, which considerably increase the effect of the surface rheology on the drainage and relaxation dynamics. For such systems our model is not applicable.

For small film thicknesses (below 200 nm) the surface forces of intermolecular origin must be accounted for. One type of such forces is the van der Waals attraction force, which is characterized by the Hamaker constant, A_H [6,47]. Many authors include the van der Waals interactions as a bulk potential force in the Navier–Stokes equation. This approach is known in the literature as the body force approach [20–26]. The body force approach applied for ionic solutions leads to very complex mathematical problems [5,16,48–51]. Many other types of surface forces are theoretically and experimentally investigated in the literature (the steric repulsion, the hydrophobic attraction, the oscillatory structural forces, etc.). In many cases the origin of the obtained interactions is not clearly understood [35,39]. For that reason, a more convenient way to account for the role of the surface forces is to use the so called disjoining pressure approach [6,47]. In this approach the bulk force density in the Navier–Stokes equation is omitted and all intermolecular interactions in the film are taken into consideration by introducing an additional disjoining pressure term, Π, in the normal stress boundary condition. The disjoining pressure depends only on the local film thickness, H, and the physicochemical properties of the solutions. The specific expressions for the different components of Π are given in Section 3. The normal component of the bulk force acting on the film surface is then compensated by the film capillary and disjoining pressures and the pressure in the gas phase, P_g. In Appendix A we derive the asymptotic form of the normal stress boundary condition. The obtained result reads

$$q+\frac{\partial w_\beta}{\partial x_\beta}+\frac{\varepsilon}{2\mathrm{Ca}}\left(\frac{\partial^2 h}{\partial x_\beta \partial x_\beta}+p_{\mathrm{dp}}-p_{\mathrm{g}}\right)=0, \tag{2.12}$$

where the capillary number, Ca, the dimensionless disjoining pressure, p_{dp}, and the pressure in the gas phase, p_{g}, are defined as follows

$$\mathrm{Ca}\equiv\frac{\eta U}{\sigma},\quad p_{\mathrm{dp}}\equiv\frac{2\Pi a^2}{\sigma b},\quad \text{and}\quad p_{\mathrm{g}}\equiv\frac{2P_{\mathrm{g}}a^2}{\sigma b}. \tag{2.13}$$

Substituting Eq. (2.12) into Eq. (2.11) we arrive to the final equation of the model:

$$\mathrm{Re}\left[\frac{\partial}{\partial t}(hw_\alpha)+\frac{\partial}{\partial x_\beta}(hw_\beta w_\alpha)\right]=\frac{\varepsilon h}{2\mathrm{Ca}}\frac{\partial}{\partial x_\alpha}\left(\frac{\partial^2 h}{\partial x_\beta \partial x_\beta}+p_{\mathrm{dp}}\right)+\frac{\partial}{\partial x_\beta}\left[h\left(\frac{\partial w_\beta}{\partial x_\alpha}+\frac{\partial w_\alpha}{\partial x_\beta}+2\frac{\partial w_\gamma}{\partial x_\gamma}\delta_{\alpha\beta}\right)\right]. \tag{2.14}$$

Note that the typical values of the capillary number are small. Thus the parameter ε/Ca in Eq. (2.14) is of the order of or larger than unity.

Erneux and Davis [22] showed that the model is analogous to a respective approach in gas dynamics. Eqs. (2.10) and (2.14) correspond to the two-dimensional viscous-flow equations if we identify the "thickness h" as the "density ρ" of the compressible gas, the "thickness h" as the "shear viscosity η". The first term in the right-hand side of Eq. (2.14) can be considered as the "pressure tensor $p_{\alpha\beta}(\rho)$", which admits the following complex "equation of state"

$$p_{\alpha\beta}(\rho)=-\frac{\varepsilon\rho}{2\mathrm{Ca}}\frac{\partial^2\rho}{\partial x_\alpha\partial x_\beta}+\frac{\varepsilon}{4\mathrm{Ca}}\left[2\int_\rho^\infty \xi\frac{\mathrm{d}p_{\mathrm{dp}}(\xi)}{\mathrm{d}\xi}\mathrm{d}\xi+\frac{\partial\rho}{\partial x_\gamma}\frac{\partial\rho}{\partial x_\gamma}\right]\delta_{\alpha\beta} \tag{2.15}$$

generalized for an arbitrary function $p_{\mathrm{dp}}(\rho)$. For small values of the film thickness, h, the "density ρ" in Eq. (2.15) is very small and the "sound speed c" becomes equal to

$$c^2=-\frac{\varepsilon\rho}{2\mathrm{Ca}}\frac{\mathrm{d}p_{\mathrm{dp}}}{\mathrm{d}\rho}. \tag{2.16}$$

Eq. (2.16) shows that if $\mathrm{d}p_{\mathrm{dp}}/\mathrm{d}\rho>0$ the "sound speed" is imaginary, which corresponds to instability. In contrast, if $\mathrm{d}p_{\mathrm{dp}}/\mathrm{d}\rho<0$ the system has a real "sound speed", corresponding to wave propagation. This fact is well known in the literature, i.e. $\mathrm{d}\Pi/\mathrm{d}H>0$ destabilizes and $\mathrm{d}\Pi/\mathrm{d}H<0$ stabilizes the drainage of thin liquid films [19].

3. One-dimensional thin liquid films attached to frames

We consider the simple case of one-dimensional thin liquid film attached to a frame (Fig. 2). The parameters of the frame are: width $2a$; left- and right-hand-side heights b_L and b, respectively. The flow rates from both frame channels are characterized by the velocities, U_L and U_R (Fig. 2), the film surfaces are symmetric with respect to the middle plane and have fixed contact lines at the frame borders. At initial time, $T=0$, the film thickness is given by the function $H_0(X)$, which determines the initial liquid volume caught in the frame. The model equations, Eqs. (2.10) and (2.14), describing the dynamics of such films, are simplified to the following:

$$\frac{\partial h}{\partial t}+\frac{\partial}{\partial x}(hw)=0, \tag{3.1}$$

$$\frac{\partial w}{\partial t}+w\frac{\partial w}{\partial x}=\frac{1}{\mathrm{We}}\frac{\partial^3 h}{\partial x^3}+\frac{4}{\mathrm{Re}}\frac{\partial^2 w}{\partial x^2}+\frac{4}{\mathrm{Re}}\frac{\partial w}{\partial x}\frac{\partial\ln h}{\partial x}+\frac{\partial}{\partial x}\left(\frac{p_{\mathrm{dp}}}{\mathrm{We}}\right), \tag{3.2}$$

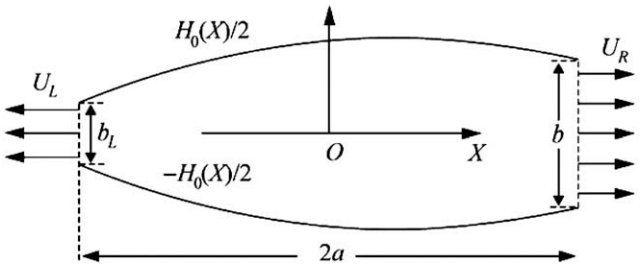

Fig. 2. Sketch of one-dimensional symmetric thin liquid film attached to a frame with a left-hand-side height b_L, right-hand-side height b, and width $2a$. The initial film thickness is $H_0(X)$, the flow rates at the left and right borders of the frame are characterized by velocities U_L and U_R, respectively.

where v is the dimensionless volume of the liquid caught in the film, per unit channel length; x, h, and w are the dimensionless lateral coordinate, thickness and velocity, respectively; and the classical Weber number is rescaled with the small parameter ε as follows

$$\mathrm{We}\equiv\frac{2}{\varepsilon}\mathrm{CaRe}=2\frac{\rho a^2U^2}{\sigma b}=\frac{2\eta^2}{\rho\sigma b}\mathrm{Re}^2. \tag{3.3}$$

At initial time, $t=0$, the liquid is at rest, the film profile is a known function, $h_0(x)$, and the liquid volume is v_0. Therefore, the initial conditions for numerical calculation of Eqs. (3.1) and (3.2) are

$$h(0,x)=h_0(x),\quad w(0,x)=0,\quad \text{and}\quad v(0)=v_0=\int_{-1}^{1}h_0(x)\mathrm{d}x. \tag{3.4}$$

The film surfaces have fixed contact lines with the frame, which assigns the following boundary conditions for the film thickness:

$$h(t,-1)=b_L/b\quad\text{and}\quad h(t,1)=1. \tag{3.5}$$

The flow rates from both sides of the frame are known (Fig. 2); they define the boundary conditions for velocity

$$w(t,-1)=-U_L(t)/U\quad\text{and}\quad w(t,1)=U_R(t)/U\quad\text{at } t>0, \tag{3.6}$$

where U is the characteristic lateral velocity (see Section 2.1). The minus sign in the first equation of Eq. (3.6) accounts for the direction of the flow (Fig. 2). In Section 4 we will study the process of film drainage to the point of minimum possible film thickness, $h_{\min}$. In this case the flow rates are non-zero during the whole process. In Section 5 the film thins under the action of the suction velocities, U_L and U_R, for a time, t_{f}, necessary to reach a given volume, v_{f}. At $t=t_{\mathrm{f}}$ suction is stopped and the film is allowed to relax to its final shape. In this case the right-hand sides of both equations in Eq. (3.6) are set to zero for $t>t_{\mathrm{f}}$, which does not change the numerical scheme described in Appendix B.

The disjoining pressure appearing in Eq. (3.2) can be presented as a sum of the van der Waals and hydrophobic attraction, Π_1, electrostatic repulsion, Π_2, steric repulsion, Π_3, and other interactions. Here we consider only the first three components: $\Pi=\Pi_1+\Pi_2+\Pi_3$. The respective dimensionless components of the disjoining pressure are denoted as p_1, p_2, and p_3. The van der Waals and hydrophobic components of the disjoining pressure are calculated by the expression $\Pi_1=-A_{\mathrm{tot}}/(6\,\pi H^3)$, where A_{tot} is an effective constant [6,47]. It is important to note that recent experiments suggest the hydrophobic interactions are in many cases stronger than the van der Waals interaction [34–38]. The authors show that the hydrophobic interactions are described by the same expression as that for the van der Waals component of the disjoining pressure, but with much larger interaction constant, K_{232}, than the Hamaker constant, A_{H}. For that reason the effective constant $A_{\mathrm{tot}}=A_H+K_{232}$ is used below. From Eqs. (2.13) and (3.3)

the attractive component of the disjoining pressure is presented in the following form:

$$\frac{p_1}{\mathrm{We}} = -\frac{B_1}{h^3} \quad \text{and} \quad B_1 \equiv \frac{A_{\mathrm{tot}}}{6\pi\rho b^3 U^2}, \tag{3.7}$$

where B_1 is the dimensionless interaction constant.

In the case of 1:1 electrolytes the electrostatic component of the disjoining pressure, Π_2, is calculated from the expression $\Pi_2 = 2E_T I(\cosh\Phi_m - 1)$, where E_T is the thermal energy, I is the ionic strength of the solution, and Φ_m is the dimensionless electric potential at the middle plane [6,47]. From Eqs. (2.13) and (3.3) we obtain the relationship between the electrostatic component of the dimensionless disjoining pressure and the dimensionless ionic strength, B_2:

$$\frac{p_2}{\mathrm{We}} = B_2(\cosh\Phi_m - 1) \quad \text{and} \quad B_2 \equiv \frac{2E_T I}{\rho U^2}. \tag{3.8}$$

It is well known in the literature [6,47] that the solution of the Poisson–Boltzmann equation for the electric potential in the film leads to the transcendental equation,

$$h = \frac{1}{\kappa b}\int_{\Phi_m}^{\Phi_s}\left(\frac{2}{\cosh\Phi - \cosh\Phi_m}\right)^{1/2} \mathrm{d}\Phi, \tag{3.9}$$

which relates the electric potential at the middle plane, Φ_m, with the surface electric potential, Φ_s, the local film thickness, h, and the Debye screening length, κ^{-1}. For a given system the surface electric potential changes insignificantly during the film drainage. Only small variations of Φ_s are possible for very thin films when the local film thickness is smaller than 10 nm [6]. Below we will assume that: (i) the constant values of Φ_s and κb are known; (ii) the numerical solution of Eq. (3.9) provides the dependence $\Phi_m = \Phi_m(h)$; (iii) Eq. (3.8) defines $p_2 = p_2(h)$. Various simpler approximations of Eqs. (3.8) and (3.9) are known in the literature [6,47]. These approximations are valid for $\kappa H \ll 1$ or $\kappa H \gg 1$ and cannot be applied for the whole film profile where H changes significantly.

The power law expressions for the steric component of the disjoining pressure, widely used in the literature [6,7,47] for protein and polymer solutions, are not consistent with our model, as seen in the discussion after Eq. (2.11). In the case of low molecular weight surfactants, the adsorbed molecules, for which our model can be applied, often possess bulky hydrophilic heads, e.g., when the polar part of the amphiphile consists of oxyethylene chains [39–41]. As the film thins, the two surfaces packed with surfactant molecules closely approach one another and the hydrophilic heads may begin to overlap. Let d be the characteristic threshold distance at which the steric interaction becomes active. The repulsive force will be described by means of a model expression for the respective disjoining pressure component, $\Pi_3 = A_{\mathrm{st}}\exp(-H/d)$, where A_{st} is the interaction constant. The validity of this asymptotic equation is discussed by many authors [7,41,47]. From Eqs. (2.13) and (3.3) one obtains the expressions for p_3 and for the interaction constant, B_3:

$$\frac{p_3}{\mathrm{We}} = B_3\exp\left(-\frac{hb}{d}\right) \quad \text{and} \quad B_3 \equiv \frac{A_{\mathrm{st}}}{\rho U^2}. \tag{3.10}$$

The nonlinear system of equations, Eqs. (3.1) and (3.2), with initial and boundary conditions, Eqs. (3.4)–(3.6), can be solved numerically by appropriate conservative finite difference scheme on staggered grids and iterative algorithms [52]. Here, we develop a faster numerical method briefly described in Appendix B. We chose a regular space and time grid with a length step, Δx, and time step, Δt. The precision of the numerical scheme (Appendix B) is $O(\Delta x^2, \Delta t^2)$, which guarantees high accuracy and efficiency of the algorithm. All calculations below are performed with $\Delta x = \Delta t = 10^{-4}$. These small values of Δx make it possible to calculate the formulated problem up to the minimum film thickness, h_{min}, of the order of or larger than 10^{-3}. More precisely, the value of h_{min} depends on the precision of the difference formula used for the first derivative of disjoining pressure, Eq. (3.7). In the case of a central difference scheme with precision $O(\Delta x^2)$ the relative error of the derivative calculated at $h_{\mathrm{min}} = 10\Delta x$ is 3.4%. This error decreases with the increase of h_{min}: for $h_{\mathrm{min}} = 20\Delta x$ the relative error is 0.84%; for $h_{\mathrm{min}} = 30\Delta x$ it is 0.37%, etc.

4. Drainage of one-dimensional thin liquid films

4.1. No disjoining pressure

When the disjoining pressure has no effect on the film dynamics, the model, given by Eqs. (3.1) and (3.2), contains two dimensionless numbers, Re and We, defined by Eqs. (2.4) and (3.3). These numbers change in a different way for given physicochemical parameters of the liquid phase depending on the velocity, U, and on the ratio b/a. For example, if for a given configuration Re = 1 and We = 1 (solid lines in Fig. 3a), then the five times increase of the velocity, U, leads to Re = 5 and We = 25 (dashed lines in Fig. 3a), while the five times decrease of U reduces these numbers to Re = 0.2 and We = 0.04 (solid lines in Fig. 3b). For a fixed value of Re the Weber number increases with the increase of

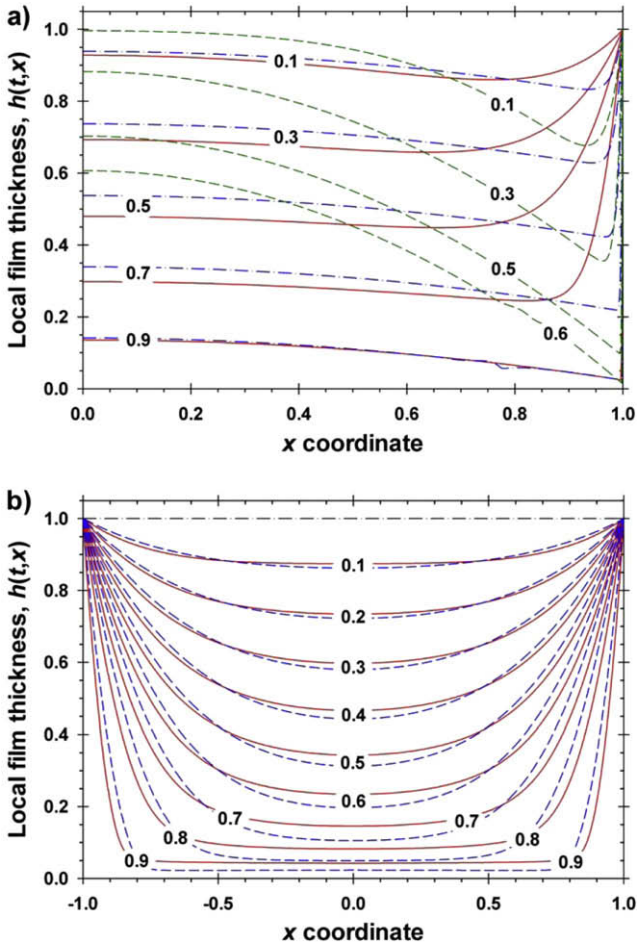

Fig. 3. Time evolution of the film profiles in the case of symmetric boundary conditions, $b_L = b$ and $U_L = U$, and an initial condition $h(x) = 1$: (a) Re = 1 and We = 1 (solid lines), Re = 1 and We = 10 (dash-dotted lines), and Re = 5 and We = 25 (dashed lines); (b) Re = 0.2 and We = 0.04 (solid lines) and Re = 1 and We = 0.1 (dashed lines).

viscosity, η, and We decreases with the increase of density, ρ, frame height, b, and surface tension, σ, see Eq. (3.3). Note that the possible changes of the surface tension of foam films are from 72 mN/m (surfactant-free systems) to 25 mN/m (close or above the critical micelle concentration), while the other parameters (η, ρ, and b) can vary in orders of magnitude. The examples for the evolution of the film profile, $h(t,x)$, in the case of Re = 1, We = 10 and Re = 1, We = 0.1 are illustrated in Fig. 3a (dash-dotted lines) and in Fig. 3b (dashed lines), respectively.

For symmetric boundary conditions, $b_L = b$ and $U_L = U$, and a constant value of the initial film thickness, $h_0(x) = 1$, the initial film volume is $v_0 = 2$ and the dimensionless time needed for the complete suction of this volume is equal to 1. For Re = 1 and We = 1 the film drains up to $t = 0.7$ without dimple formation and with a virtually fixed length of its plane-parallel region (Fig. 3a – solid lines). Subsequently the film ring spreads to the borders, a pronounced dimple is formed, and at $t = 0.9$ the film ruptures because the menisci at the film periphery "touch" the frame borders. Therefore, the rupture is not a result of reaching the minimal possible thickness, h_{min}. With the five times increase of the flow rate a well pronounced dimple is formed at an early stage, the dimple grows, the film ring spreads, and at $t = 0.6$ the film ruptures before reaching h_{min} (Fig. 3a – dashed lines). At the final moment the dimple height at $x = 0$ has quite a large value of 0.6, thus the dimple covers 40% of the initial film volume. Increasing the Weber number (Re = 1 and We = 10) results in the film surfaces becoming more deformable (Fig. 3a – dash-dotted lines). In this case the evolution of $h(t,x)$ is similar to the case with the ten times smaller Weber number: the thicknesses of the two films at $x = 0$ are close to each other; the film ring for We = 10 is initially larger than that for We = 1, but at the final stage both film profiles are virtually identical. Therefore, the Weber number can be considered as a characteristic of the deformability of film surfaces.

From a practical viewpoint it is very important to produce films with thickness as uniform as possible and with a large plane-parallel area. One way is to reduce the flow rate: as it is shown in Fig. 3b (solid lines), the five times decrease of the flow rate (Re = 0.2, We = 0.04) leads to a regular film thinning with a continuous increase of the plane-parallel region up to $t = 0.9$ when the film thickness at $x = 0$ is 4.25×10^{-2} and the film ring is placed approximately at $x \approx 0.8$. Another way is to decrease the deformability of film surfaces: for Re = 1 the ten times decrease of the Weber number, We = 0.1, stabilizes the process of film drainage (Fig. 3b – dashed lines). Such films have regular profiles, $h(t,x)$, during the whole process. At moment $t = 0.9$ their thickness at $x = 0$ is 2.31×10^{-2}, i.e. smaller than that for the case of Re = 0.2 and We = 0.04, and the film ring is placed approximately at the same place $x \approx 0.8$.

In the case of unsymmetrical boundary conditions the production of films with large plane-parallel areas is a more complicated task. One can expect that the increase of the surface tension will help to solve this problem. Our calculations for Re = 1, We = 0.1, $b_L = b$, $h_0(x) = 1$, and without a liquid flow from the left-hand-side boundary (Fig. 4a) show that in this case a dimple does not form, i.e. a large amount of liquid is left captured close to the left-hand-side boundary. Because of the twice smaller flow rate (only from one side) the dimensionless time necessary for the complete suction of the initial volume is equal to 2. The film reaches its minimal thickness slightly after $t = 1.4$ with a complex shape without plane-parallel regions. The minimal film thickness is located at $x = 0.75$. The process of film drainage is regular, without waves and instabilities. We have performed calculations for the same case decreasing the Weber number to We = 0.01. The film profile at the moment of reaching of h_{min} is plotted in Fig. 4a (dashed line), where it can be seen that h_{min} is located at $x = 0.38$. The following conclusions can be drawn: these films reach the minimal thickness

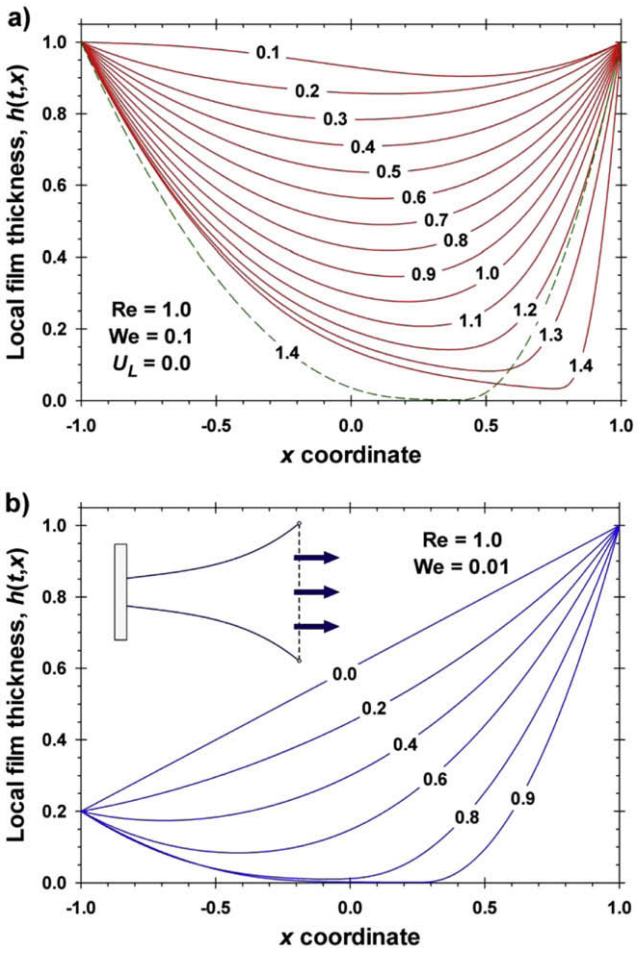

Fig. 4. Plots of $h(t,x)$ for film drainage in the absence of a flow from the left-hand-side border: (a) $b_L = b$ and initial condition $h_0(x) = 1$ at Re = 1, We = 0.1, till $t = 1.4$ (solid lines) and at Re = 1, We = 0.01, $t = 1.4$ (dashed line); (b) Re = 1, We = 0.01, $b_L/b = 0.2$, and initial condition $h_0(x) = 0.6 + 0.4x$.

at approximately the same time; the decrease of deformability of film surfaces leads to more symmetric film thicknesses but the plane-parallel areas of the films are very small for unsymmetrical boundary conditions.

To extend the plane-parallel film region we have decreased five times the height of the left-hand-side border assuming that $b_L/b = 0.2$ and have used the same conditions as in Fig. 4a with a smaller value of the Weber number, We = 0.01 (Fig. 4b). Starting with an initial condition, $h_0(x) = 0.6 + 0.4x$, corresponding to an initial dimensionless volume, $v_0 = 1.2$, we have obtained that the evolution of such films is regular until the minimal film thickness, h_{min}, is reached at $t = 0.9$ and $x = 0.23$. Therefore, the considerable decrease of the deformability of film surfaces and the frame height, b_L, is not sufficient to produce large plane-parallel film areas. The calculations illustrated in Figs. 3 and 4 show that the most efficient way to accomplish this technological task is to use symmetric flow rates and symmetric geometrical parameters of the frames as much as possible.

4.2. Effect of van der Waals and hydrophobic attraction

The van der Waals and hydrophobic attractions, accounted for by the disjoining pressure component Π_1, are always active and have the longest range compared to the other components of Π. The role of this kind of attraction forces on the evolution of the film profiles in the case of symmetric boundary conditions for Re = 1,

We = 1, and $B_1 = 0.1$ is illustrated in Fig. 5a (solid lines). The comparison between Figs. 3a and 5a (solid lines) shows that up to time $t = 0.7$ the disjoining pressure does not considerably affect the process of the film drainage. When the local film thickness decreases to a certain critical value, the attraction forces become significant and the area of the film ring thins faster. At time $t = 0.818$ the film reaches $h_{\min}$ at position $x = 0.984$ and breaks. The final dimple covers 1.82% of the initial liquid volume. One expects that the decrease of the flow rate always makes the film drainage more regular (see Fig. 3). When keeping all the other parameters constant and decreasing five times the flow rate, the value of B_1 increases 25 times, see Eq. (3.7). The obtained numerical results for Re = 0.2, We = 0.04, and $B_1 = 2.5$ are plotted in Fig. 5a (dashed lines). The comparison of these results with those plotted in Fig. 3b (solid lines) in the case without disjoining pressure taken into account shows that both films follow the same regular behavior up to time $t = 0.4$. At subsequent moments the attraction molecular forces significantly accelerate the film thinning in the central zone, $x = 0$ (compare the respective profiles for $t = 0.5$, 0.55, 0.58, and 0.591). At $t = 0.591$ a typical instability appears and the film breaks. This effect is known in the literature as "pimple" formation as opposed to the case of the film breakage at the ring [53].

4.3. Effect of electrostatic and steric repulsion

One possibility to reduce the destabilizing role of the attractive components of the disjoining pressure is to use ionic surfactants

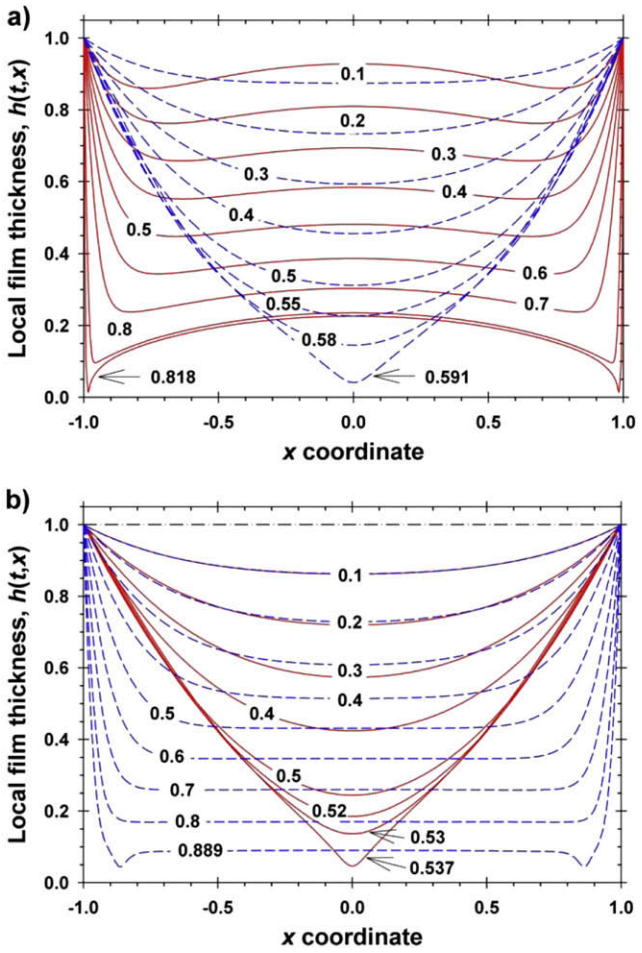

Fig. 5. Role of disjoining pressure on the drainage of films with symmetric boundary conditions and initial condition $h_0(x) = 1$: (a) Re = 1, We = 1, $B_1 = 0.1$ (solid lines) and Re = 0.2, We = 0.04, $B_1 = 2.5$ (dashed lines); (b) Re = 1, We = 0.1, $B_1 = 1$ (solid lines) and additionally $B_{el} = 10^4$, and $\kappa b = 10$ (dashed lines).

and thus increase the electrostatic component of Π. It is proven in the literature that even without added surfactants the surface potential is different from zero: its origin for such systems is the surface charge due to the spontaneous adsorption of hydroxyl ions [32,33]. In the case of large values of κH the asymptotic expression for the electrostatic component of the disjoining pressure, Π_2, reads $\Pi_2 = 64E_T I\tanh^2(\Phi_s/4)\exp(-\kappa H)$ [6]. Therefore, a more convenient dimensionless parameter, characterizing the magnitude of this force is $B_{\rm el} \equiv 32B_2\tanh^2(\Phi_s/4)$, see Eq. (3.8). In Fig. 3b (dashed lines) we have illustrated that at Re = 1 the decrease of the Weber number to We = 0.1 leads to a regular drainage of such films. If we take into account the action of the attractive component of the disjoining pressure by assuming that $B_1 = 1$ and calculate the film evolution, we obtain the solid lines in Fig. 5b. It is clearly seen that after $t = 0.4$ the profiles $h(t,x)$ accelerate in time, at $t = 0.537$ a pimple instability appears at the central zone and subsequently the film breaks. Note that the film in Fig. 3b obtained at the same process parameters but without the action of Π_1 has a wide plane-parallel region at $t = 0.9$. In order to have an idea about the magnitude of $B_{\rm el}$ one calculates its value for water solution without surfactants at pH = 9 and room temperature: $B_{\rm el} = 45a^2/(b\mathrm{We})$. Taking the values We = 0.1, $b = 1$ μm, and $a = 5$ mm we obtain that $B_{\rm el} = 1.1 \times 10^4$ and the respective value of κb is 10.3. Experiments for film drainage and equilibrium thickness of similar systems are reported in Ref. [54]. The increase of the surface potential and ionic strength increases $B_{\rm el}$ and κb. The film, which is unstable without accounting for the electrostatic repulsion, becomes more stable for $B_{\rm el} = 10^4$ and $\kappa b = 10$, see Fig. 5b (dashed lines). The comparison between Figs. 3b and 5b (dashed lines) shows that in the presence of disjoining pressure the electrostatic repulsion counterbalances the attraction forces in a wide plane-parallel central zone. Nevertheless, at the latest stage of film drainage a well pronounced film ring at $x = 0.864$ is formed and subsequently the film breaks down.

The decrease of the surface potential, Φ_s, suppresses the electrostatic interactions. For example, if we take the above system and change pH to 5 while keeping all the other parameters constants, the value of $B_{\rm el}$ decreases ten times. The smaller repulsive force is not sufficient to prevent the pimple formation, see Fig. 6 (solid line). The comparison between Figs. 5b and 6 (solid lines) illustrates that the electrostatic component of Π decelerates the appearance of such kind of instabilities. The film (Fig. 6, solid line) thins regularly for a longer time $t = 0.65$ compared to that without Π_2, which thins in a similar manner up to $t = 0.52$ (Fig. 5b, solid line). Nevertheless, at $t = 0.682$ (Fig. 6, solid lines) the attractive components of the disjoining pressure prevail and the film ruptures at its center line. In addition, the shorter range repulsive force can be included, namely the effect of steric interactions can be investigated. As a rule [39–41] for such forces b/d is much larger than κb, except for the cases of large ionic strengths, and the interaction constant, $A_{\rm st}$, is very large, see Eq. (3.10). In Fig. 6 (dashed lines) we calculate the film evolution additionally accounting for the steric interactions at $b/d = 20$ and $B_3 = 3 \times 10^4$. In this case the drainage process stabilizes and regular film thinning is observed up to $t = 0.9$. The mechanism of the film rupture changes to a ring formation at position and time, $x = 0.916$ and $t = 0.921$, respectively, and a large plane-parallel central zone with thickness 0.064 is formed. Figs. 5b and 6 show that the dynamic effects cannot be suppressed by the action of the repulsive disjoining pressure.

5. Relaxation of one-dimensional thin liquid films

If one wants to produce a film with a given volume, v_f, the flow rates are stopped after time, t_f. Depending on the magnitudes of

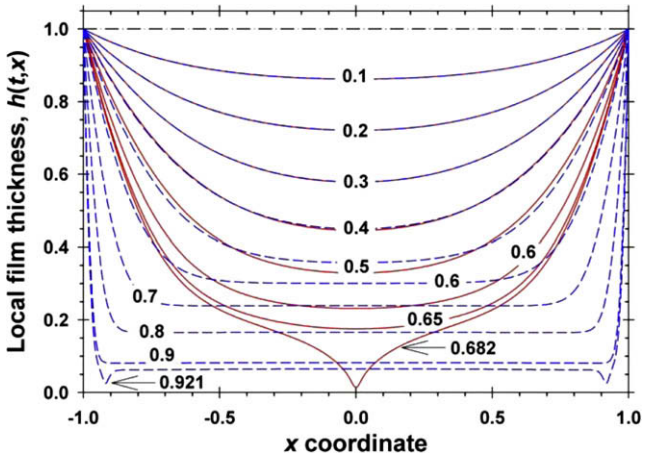

Fig. 6. Role of electrostatic and steric components of the disjoining pressure for the drainage of films with symmetric boundary conditions and initial condition $h_0(x) = 1$ for Re = 1, We = 0.1, $B_1 = 1$, $B_{el} = 10^3$ and $\kappa b = 10$ (solid lines), and additionally $B_3 = 3 \times 10^4$ and $b/d = 20$ (dashed lines).

interaction forces and regimes of film drainage the film surfaces will relax to the steady state film profile, $h_{st}(x)$, or eventually the film may rupture before reaching $h_{st}(x)$ (see below). In the case of thick films when the role of the disjoining pressure can be neglected, the static variant of Eq. (3.2), simplifies to $d^3h_{st}(x)/dx^3 = 0$. The solution for films with symmetric boundary conditions, $h_{st}(\pm 1) = 1$, and a fixed volume, v_f, is

$$h_{st}(x) = \frac{3v_f - 2}{4} + \frac{6 - 3v_f}{4}x^2. \tag{5.1}$$

Therefore, the minimum possible dimensionless volume (minimum static equilibrium volume) is 2/3 and if $v_f < 2/3$ the Laplace equation of capillarity has no solution, thus no static equilibrium exists. Therefore, if one stops the flow rates at $t_f > 2/3$ in the case shown in Fig. 3 the respective films will break. When the disjoining pressure is taken into account, the static variant of Eq. (3.2) has no analytical solution and $h_{st}(x)$ is obtained as a limit of $h(t,x)$ after complete relaxation.

The first step in our study is to obtain the characteristic relaxation time and the type of film profile relaxation in the simplest case, without the disjoining pressure effect being taken into account. We consider two cases for Re = 1, We = 1, and volume $v_f = 1$, larger than the minimum possible one, 2/3: initial film profile is $h_0(x) = 1$ (flat surfaces) and $t_f = 0.5$, and parabolic initial profile, $h_0(x) = (5+3x^2)/8$ with $v_0 = 1.5$ and $t_f = 0.25$ (Fig. 7). The drainage of these films is illustrated in Fig. 3a (solid lines) and Fig. 7a (dashed lines); the respective relaxation curves show a similar behavior. The solid lines in Fig. 7a show the evolution of film profiles, $h(t,x)$, during the process of relaxation for $t > t_f$. The stable regular approach to the equilibrium state $h_{st}(x) = (1 + 3x^2)/4$ is well illustrated. The changes of the thickness difference, $h(t,x) - h_{st}(x)$, with time for both sets of initial conditions are shown in Fig. 7b. One sees that in these cases the initial conditions do not affect the type of relaxation for all values of the lateral coordinate. In the inset of Fig. 7b we present the changes of thickness difference in the central zone, $h(t,0) - h_{st}(0)$, in a logarithmic scale as a function of $t - t_f$. The excellent parallel straight lines with a slope of -1.5 proves that the relaxation obeys an exponential rule, $\propto \exp(-1.5t)$, for both kinds of initial conditions. Therefore, the elastic force arising from the action of the surface tension is strong enough to stabilize such films.

The attraction component of the disjoining pressure destabilizes the films not only in the film drainage process (see Fig. 5a), but also during the film relaxation. If we take the films given in

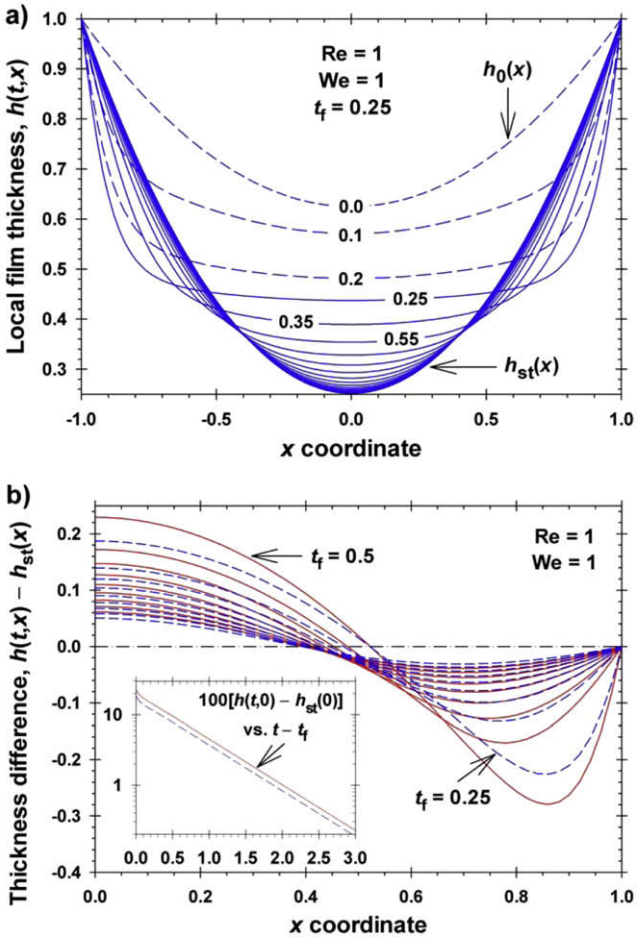

Fig. 7. Relaxation of films for Re = 1, We = 1, and $v_f = 1$: (a) Local film thickness, $h(t,x)$, with initial profile, $h_0(x) = (5 + 3x^2)/8$, and initial volume, $v_0 = 1.5$, $t_f = 0.25$ (solid lines). For $t > 0.35$ solid lines correspond to time step 0.2; (b) thickness difference, $h(t,x) - h_{st}(x)$, lines plotted with time step 0.1 for $h_0(x) = 1$, $v_0 = 2$, $t_f = 0.5$ (solid lines) and for case (a) (dashed lines). The inset shows the difference $h(t,0) - h_{st}(0)$ in time, $t - t_f$, for the two cases after the film suction is stopped.

Fig. 5a and stop the flow rates at $t_f = 0.45$, when the liquid volume $v_f = 1.1$ is larger than that for the films in Fig. 7, the films cannot reach the steady state and therefore rupture, as seen on Fig. 8. In the case of Re = 1, We = 1, and $B_1 = 0.1$ the change of $h(t,x)$ for $t \geqslant 0.45$ with a time step 0.1 is shown in Fig. 8. The pimple type instability appears at $t = 2.245$ and subsequently the film ruptures in its central zone. The inset of Fig. 8 demonstrates the decrease of $h(t,0)$ with time for this film (solid line) and for the film with the same physicochemical parameters, but with 5 times smaller suction velocity (dashed line). One sees that in both cases the instability appears at $x = 0$ and for smaller flow rates the dimensionless rupture time of 0.707 for Re = 0.2 is lower than that of 2.245 for Re = 1. Taking into account the definition, Eq. (2.1), one concludes that due to the 5 times smaller flow rate the real rupture time, T, for Re = 0.2 becomes longer ($5 \times 0.707 = 3.535$) than that for Re = 1. This fact can be explained by the longer time needed to suppress the larger local surface velocities after stopping the film drainage at larger flow rates.

As discussed above, the production of plane-parallel films with small volumes, $v_f < 2/3$, and thicknesses is impossible without using additives, which increase the repulsive components of the disjoining pressure. However, the attractive disjoining pressure always appears and cannot be excluded from consideration. The dashed lines in Figs. 5b and 6 represent regular film drainage in

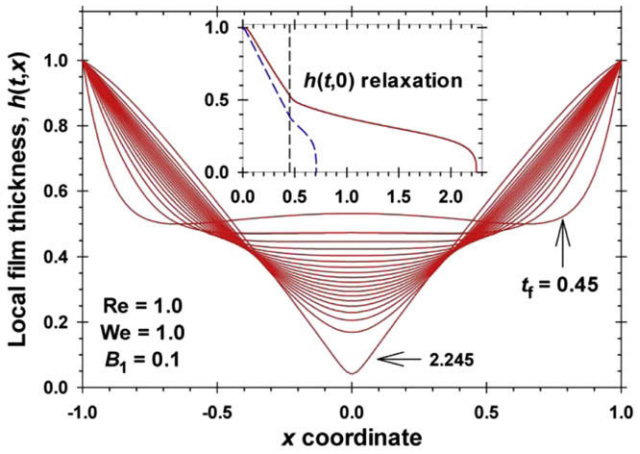

Fig. 8. Relaxation of film surfaces in the case of symmetric boundary conditions for Re = 1, We = 1, $B_1 = 0.1$, and $t_f = 0.45$. Solid lines are plotted with time step 0.1 and the moment before the film rupture is 2.245. The inset compares the relaxation of $h(t,0)$ for this film (solid line) with the case of relaxation of the same film but with five times smaller flow rate Re = 0.2, We = 0.04, $B_1 = 2.5$, and $t_f = 0.45$ (dashed line).

the presence of Π_2 and Π_3. We took these systems and stopped the flow rates at two different times, at $t = 0.7$ when $v_f = 0.6$, and at $t = 0.85$ when the volume is smaller, $v_f = 0.3$. For both systems and times the final film profiles, $h_{st}(x)$, are shown in Fig. 9. One sees that the films contain large almost plane-parallel central zones and steep menisci around them. These films are stable because the repulsive components of the disjoining pressure, Π_2 and Π_3, prevail the respective van der Waals and hydrophobic components, Π_1. The inset of Fig. 9 illustrates the type of relaxation of these films – in all cases the film thickness, $h(t,0)$, for $t > t_f$ oscillates around the equilibrium thickness, $h_{st}(0)$, but the amplitudes of oscillations exponentially decrease with time. By applying linear stability analysis, analogous to that given in Ref. [23], for the disturbances of the film surfaces in a central plane-parallel zone one proves that the critical wavelengths for the cases illustrated in Fig. 9 are much larger than the lateral dimension of the frame. Therefore, the final film thicknesses correspond to a stable equilibrium.

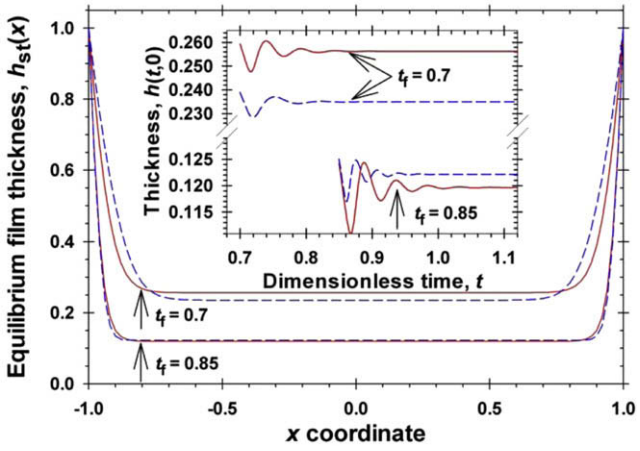

Fig. 9. Equilibrium film thicknesses for Re = 1, We = 0.1, and $B_1 = 1$ corresponding to $t_f = 0.7$ and $t_f = 0.85$. Solid lines are plotted for $B_{el} = 10^4$ and $\kappa b = 10$ without accounting for the steric interactions (see Fig. 5b) and dashed lines – for $B_{el} = 10^3$, $\kappa b = 10$, $B_3 = 3 \times 10^4$, and $b/d = 20$ (see Fig. 6). The inset illustrates the respective relaxations of $h(t,0)$ after stopping the flow rates.

These conclusions are important for practical applications because they give one possible way for a controllable production of large thin films.

6. Summary and conclusions

A model describing the drainage and relaxation dynamics of symmetric thin liquid films with tangentially mobile surfaces is developed. The obtained equations, Eqs. (2.10)–(2.12), are applicable for laminar flows when the film thicknesses are much smaller than the characteristic lateral dimensions. The model describes the film profile, surface velocity and pressure for arbitrary values of the Reynolds and capillary number, accounting for different components of the disjoining pressure. In the case of one-dimensional film attached to a frame the problem is simplified in Section 3 and the van der Waals, hydrophobic, electrostatic and steric interactions between film surfaces are included in the disjoining pressure. A fast algorithm for numerical solution of this problem, which has a second order precision in time and space, is developed in Appendix B and applied in Sections 4 and 5.

In the case of unsymmetrical boundary conditions (different flow rates or frame heights) the films drain with complex shapes of their surfaces, therefore the formation of large plane-parallel areas by controlling the flow rates is difficult (Fig. 4). For films with symmetrical boundary conditions the increase of flow rates leads to a pronounced dimple formation with a ring close to the frame (Fig. 3a). The process of film drainage becomes more regular with almost no dimple formation by decreasing the flow rate or the deformability of the film surfaces, i.e. for smaller values of the Reynolds and Weber numbers (Fig. 3b). The attractive disjoining pressure favors the film breakage in two different ways: for larger flow rates the dimple ruptures at its ring; for smaller flow rates the film breaks in its central zone (Fig. 5). The electrostatic and steric repulsive components of the disjoining pressure can suppress the van der Waals and hydrophobic attraction, making the process of film drainage regular, with a wide central plane-parallel zone (Figs. 5 and 6). The type of film drainage can be efficiently controlled by varying the magnitudes of different components of the disjoining pressure.

When the flow rates are stopped, the film surfaces either relax to their final equilibrium profile, or the film ruptures. For a given liquid volume the Laplace equation of capillarity describes the steady film thickness, $h_{st}(x)$. Without accounting for the repulsive components of the disjoining pressure, $h_{st}(x)$ has a parabolic or pimple form without plane-parallel areas. The films can be either stable with an exponential decay of surface corrugations (Fig. 7) or unstable if attractive surface forces are present (Fig. 8). The only possible way to produce films with small volumes and thicknesses is to control the magnitudes of electrostatic and steric interactions (Fig. 9). These films are stable: their thicknesses oscillate around the equilibrium profiles, $h_{st}(x)$, and the amplitudes of surface corrugations exponentially decrease with time. The equilibrium profiles contain large almost plane-parallel central zones and steep menisci close to the frames.

The model described in Section 2 can be applied to study the drainage and relaxation dynamics of circular films. However in this case the films thin under the action of a constant pressure difference, which changes the boundary conditions. The change of geometry and boundary conditions must be taken into account in the model equations and numerical scheme. This problem is an aim for our future publication.

Acknowledgment

This study is partially funded by project INZ01/01024 of the National Science Fund of Bulgaria (program "Integrated Research Centers in the Universities").

Appendix A. Derivation of the leading order of the dynamic boundary conditions at the film surface

To obtain the density of the force, $\mathbf{F}_s$, acting from the bulk fluid onto the upper film interface one needs to calculate the normal projection of the bulk stress tensor, $\mathbf{P}$, at the surface. We will use the following notations: $\mathbf{e}_k$ ($k = 1, 2, 3$) are the unit vectors of the Cartesian coordinate systems $OX_1X_2X_3$; $\mathbf{t}_\alpha$ ($\alpha = 1, 2$) are the tangential vectors at the upper film surface; $\mathbf{n}$ is the respective surface normal vector. Therefore,

$$\mathbf{t}_\alpha = \left(\mathbf{e}_\alpha + \frac{1}{2}\frac{\partial H}{\partial X_\alpha}\mathbf{e}_3\right)\left[1 + \left(\frac{1}{2}\frac{\partial H}{\partial X_\alpha}\right)^2\right]^{-1/2} \quad (\alpha = 1, 2), \tag{A.1}$$

$$\mathbf{n} = \left(-\frac{1}{2}\frac{\partial H}{\partial X_\beta}\mathbf{e}_\beta + \mathbf{e}_3\right)\left[1 + \left(\frac{1}{2}\frac{\partial H}{\partial X_1}\right)^2 + \left(\frac{1}{2}\frac{\partial H}{\partial X_2}\right)^2\right]^{-1/2}. \tag{A.2}$$

For incompressible Newtonian fluids the stress tensor, $\mathbf{P}$, is given by the definition [42]

$$P_{ik} = P\delta_{ik} - \eta\left(\frac{\partial U_i}{\partial X_k} + \frac{\partial U_k}{\partial X_i}\right), \tag{A.3}$$

where δ_{ik} is the Kronecker delta. From Eqs. (A.1)–(A.3) one derives the expression for the force density, $\mathbf{F}_s = \mathbf{P}\cdot\mathbf{n}$:

$$\mathbf{F}_s\cdot\mathbf{e}_k = \left(-\frac{P_{k\beta}}{2}\frac{\partial H}{\partial X_\beta} + P_{k3}\right)\left[1 + \left(\frac{1}{2}\frac{\partial H}{\partial X_1}\right)^2 + \left(\frac{1}{2}\frac{\partial H}{\partial X_2}\right)^2\right]^{-1/2}, \tag{A.4}$$

where all parameters are calculated at $X_3 = H/2$ and $k = 1, 2, 3$.

From Eqs. (A.1) and (A.4) we obtain the formula for the tangential component of the force:

$$\begin{aligned}\mathbf{F}_s\cdot\mathbf{t}_\alpha = {}& \left(P_{\alpha 3} + \frac{P_{33}}{2}\frac{\partial H}{\partial X_\alpha} - \frac{P_{\alpha\beta}}{2}\frac{\partial H}{\partial X_\beta} - \frac{P_{3\beta}}{4}\frac{\partial H}{\partial X_\beta}\frac{\partial H}{\partial X_\alpha}\right)\\ &\times\left[1 + \left(\frac{1}{2}\frac{\partial H}{\partial X_1}\right)^2 + \left(\frac{1}{2}\frac{\partial H}{\partial X_2}\right)^2\right]^{-1/2}\\ &\times\left[1 + \left(\frac{1}{2}\frac{\partial H}{\partial X_\alpha}\right)^2\right]^{-1/2} \quad \text{at } X_3 = \frac{H}{2}.\end{aligned} \tag{A.5}$$

The tangential stress boundary condition (see Section 2.2) for free surfaces reads $\mathbf{F}_s\cdot\mathbf{t}_\alpha = 0$. Substituting the definition of the stress tensor, Eq. (A.3), into Eq. (A.5) one reduces the tangential stress boundary condition to the following relationship

$$\begin{aligned}&4\left(\frac{\partial U_\alpha}{\partial X_3} + \frac{\partial U_3}{\partial X_\alpha}\right) + 4\frac{\partial U_3}{\partial X_3}\frac{\partial H}{\partial X_\alpha} - 2\left(\frac{\partial U_\alpha}{\partial X_\beta} + \frac{\partial U_\beta}{\partial X_\alpha}\right)\frac{\partial H}{\partial X_\beta}\\ &- \left(\frac{\partial U_3}{\partial X_\beta} + \frac{\partial U_\beta}{\partial X_3}\right)\frac{\partial H}{\partial X_\beta}\frac{\partial H}{\partial X_\alpha} = 0 \quad \text{at } X_3 = \frac{H}{2}.\end{aligned} \tag{A.6}$$

From Eqs. (2.1),(2.2) and (A.6) we obtain the dimensionless form of this boundary condition:

$$\begin{aligned}\frac{1}{\varepsilon^2}\frac{\partial u_\alpha}{\partial x_3} = {}& -\frac{\partial u_3}{\partial x_\alpha} - \frac{\partial u_3}{\partial x_3}\frac{\partial h}{\partial x_\alpha} + \frac{1}{2}\left(\frac{\partial u_\alpha}{\partial x_\beta} + \frac{\partial u_\beta}{\partial x_\alpha}\right)\frac{\partial h}{\partial x_\beta}\\ &+ \frac{1}{4}\left(\varepsilon^2\frac{\partial u_3}{\partial x_\beta} + \frac{\partial u_\beta}{\partial x_3}\right)\frac{\partial h}{\partial x_\beta}\frac{\partial h}{\partial x_\alpha} \quad \text{at } x_3 = \frac{h}{2}.\end{aligned} \tag{A.7}$$

Using the leading order solution of the considered problem, Eqs. (2.7) and (2.8), we simplify the right-hand side of Eq. (A.7) to the asymptotic expression:

$$\left.\frac{1}{\varepsilon^2}\frac{\partial u_\alpha}{\partial x_3}\right|_{x_3 = h/2} = \frac{h}{2}\frac{\partial^2 w_\beta}{\partial x_\alpha \partial x_\beta} + \frac{\partial h}{\partial x_\alpha}\frac{\partial w_\beta}{\partial x_\beta} + \frac{1}{2}\left(\frac{\partial w_\alpha}{\partial x_\beta} + \frac{\partial w_\beta}{\partial x_\alpha}\right)\frac{\partial h}{\partial x_\beta} + O(\varepsilon^2). \tag{A.8}$$

Substituting Eq. (2.7) into Eq. (2.5) we reduce it to the asymptotic relationship:

$$\begin{aligned}\frac{1}{\varepsilon^2}\frac{\partial^2 u_\alpha}{\partial x_3^2} = {}& \frac{\partial}{\partial x_\alpha}\left(q - \frac{\partial w_\beta}{\partial x_\beta}\right) - \frac{\partial^2 w_\alpha}{\partial x_\beta \partial x_\beta}\\ &+ \mathrm{Re}\left[\frac{\partial w_\alpha}{\partial t} + \frac{\partial}{\partial x_\beta}(w_\beta w_\alpha) + \frac{\partial}{\partial x_3}(u_3 w_\alpha)\right] + O(\varepsilon^2).\end{aligned} \tag{A.9}$$

Integrating Eq. (A.9) with respect to x_3 from 0 to $h/2$ and accounting for the kinematic boundary condition, Eq. (2.9), one derives

$$\begin{aligned}\left.\frac{1}{\varepsilon^2}\frac{\partial u_\alpha}{\partial x_3}\right|_{x_3 = h/2} = {}& \frac{h}{2}\frac{\partial q}{\partial x_\alpha} - \frac{h}{2}\frac{\partial^2 w_\beta}{\partial x_\alpha \partial x_\beta} - \frac{h}{2}\frac{\partial^2 w_\alpha}{\partial x_\beta \partial x_\beta}\\ &+ \mathrm{Re}\left[\frac{\partial}{\partial t}\left(\frac{h}{2}w_\alpha\right) + \frac{\partial}{\partial x_\beta}\left(\frac{h}{2}w_\beta w_\alpha\right)\right] + O(\varepsilon^2).\end{aligned} \tag{A.10}$$

Therefore, the right-hand sides of Eqs. (A.8) and (A.10) must be equal and after simple transformations we arrive to the result given by Eq. (2.11) in Section 2.2.

From Eqs. (A.2) and (A.4) one calculates the expression for the normal component of the force density:

$$\begin{aligned}\mathbf{F}_s\cdot\mathbf{n} = {}& \left(\frac{P_{\alpha\beta}}{4}\frac{\partial H}{\partial X_\alpha}\frac{\partial H}{\partial X_\beta} - \frac{\partial H}{\partial X_\beta}P_{\beta 3} + P_{33}\right)\\ &\times\left[1 + \left(\frac{1}{2}\frac{\partial H}{\partial X_1}\right)^2 + \left(\frac{1}{2}\frac{\partial H}{\partial X_2}\right)^2\right]^{-1},\end{aligned} \tag{A.11}$$

where all parameters are calculated at $X_3 = H/2$. By substituting the definitions of the stress tensor, Eq. (A.3), and of the dimensionless parameters, Eqs. (2.1), (2.2) and (2.4), in Eq. (A.11) we derive the relationship

$$\begin{aligned}\mathbf{F}_s\cdot\mathbf{n} = {}& \frac{\eta U}{a}p + \frac{\eta U}{a}\left[2\frac{\partial u_\beta}{\partial x_\beta} + \frac{\partial h}{\partial x_\beta}\frac{\partial u_\beta}{\partial x_3} + \varepsilon^2\frac{\partial h}{\partial x_\beta}\frac{\partial u_3}{\partial x_\beta}\right.\\ &\left.- \frac{\varepsilon^2}{4}\left(\frac{\partial u_\alpha}{\partial x_\beta} + \frac{\partial u_\beta}{\partial x_\alpha}\right)\frac{\partial h}{\partial x_\alpha}\frac{\partial h}{\partial x_\beta}\right]\left[1 + \varepsilon^2\left(\frac{1}{2}\frac{\partial h}{\partial x_1}\right)^2 + \varepsilon^2\left(\frac{1}{2}\frac{\partial h}{\partial x_2}\right)^2\right]^{-1}\end{aligned} \tag{A.12}$$

written at $x_3 = h/2$.

From the leading order solution, Eq. (2.7), the tangential stress boundary condition, Eq. (A.8), and Eq. (A.12) one obtains:

$$\mathbf{F}_s\cdot\mathbf{n} = \frac{\eta U}{a}\left[q + \frac{\partial w_\beta}{\partial x_\beta} + O(\varepsilon^2)\right]. \tag{A.13}$$

The normal stress boundary condition reads (see Section 2.2 and [55])

$$\mathbf{F}_s\cdot\mathbf{n} + P_c + \Pi = P_g, \tag{A.14}$$

where P_g is the pressure in the gas phase, P_c is the film capillary pressure, and Π is the disjoining pressure. From Eqs. (A.13) and (A.14) the leading order form of the normal stress boundary condition is reduced to

$$q + \frac{\partial w_\beta}{\partial x_\beta} + \frac{\sigma b}{2\eta U a}\left(\frac{\partial^2 h}{\partial x_\beta \partial x_\beta} + \frac{2\Pi a^2}{\sigma b} - \frac{2P_g a^2}{\sigma b}\right) = 0. \tag{A.15}$$

By defining the capillary number and the dimensionless disjoining and gas pressures by Eq. (2.13) we transform Eq. (A.15) into the final result given by Eq. (2.12).

Appendix B. Numerical scheme

To construct the numerical scheme we denote the values of all parameters at time t with the superscript (-) and those calculated at time $t + \Delta t$ with the superscript (+), where Δt is the local numerical time step. For example, $h^{(-)}$ and $w^{(-)}$ are taken at time level t,

while $h^{(+)}$ and $w^{(+)}$ – at the subsequent time level $t + \Delta t$. The respective time differences, Δh and Δw, are defined as $\Delta h \equiv h^{(+)} - h^{(-)}$ and $\Delta w \equiv w^{(+)} - w^{(-)}$. Eqs. (3.1) and (3.2) are considered at moment $t + \Delta t/2$ and the time derivatives appearing therein are approximated with precision Δt^2:

$$\frac{\Delta h}{\Delta t} = R_h|_{t+\Delta t/2} + O(\Delta t^2) \quad \text{and} \quad \frac{\Delta w}{\Delta t} = R_w|_{t+\Delta t/2} + O(\Delta t^2), \tag{B.1}$$

where the operators, R_h and R_w, are defined by the expressions

$$R_h \equiv -\frac{\partial}{\partial x}(hw), \tag{B.2}$$

$$R_w \equiv -\frac{\partial}{\partial x}\left(\frac{w^2}{2}\right) + \frac{1}{\mathrm{We}}\frac{\partial^3 h}{\partial x^3} + \frac{\partial}{\partial x}\left(\frac{p_{\mathrm{dp}}}{\mathrm{We}}\right) + \frac{4}{\mathrm{Re}}\frac{\partial^2 w}{\partial x^2} + \frac{4}{\mathrm{Re}}\frac{\partial w}{\partial x}\frac{\partial \ln h}{\partial x}. \tag{B.3}$$

Using the Crank-Nicolson method [56,57] the right-hand sides of the equations in Eq. (B.1) are replaced with the mean values of operators at time levels t and $t + \Delta t$ with accuracy $O(\Delta t^2)$, i.e.

$$\frac{\Delta h}{\Delta t} - \frac{R_h^{(+)} - R_h^{(-)}}{2} = R_h^{(-)} + O(\Delta t^2) \quad \text{and}$$
$$\frac{\Delta w}{\Delta t} - \frac{R_w^{(+)} - R_w^{(-)}}{2} = R_w^{(-)} + O(\Delta t^2). \tag{B.4}$$

In order to apply the Newton method for linearization [56,57] we calculate the variations of $R_h^{(+)} - R_h^{(-)}$ and $R_w^{(+)} - R_w^{(-)}$ with second order precision $O(\Delta h^2, \Delta w^2)$ using the above definitions, Eqs. (B.2) and (B.3). After simple transformations one arrives to the relationships

$$\frac{\Delta h}{\Delta t} + \frac{1}{2}\frac{\partial}{\partial x}[h^{(-)}\Delta w + w^{(-)}\Delta h] = R_h^{(-)}, \tag{B.5}$$

$$\frac{\Delta w}{\Delta t} + \frac{\partial}{\partial x}\left[\frac{w^{(-)}\Delta w}{2}\right] - \frac{1}{2We}\frac{\partial^3 \Delta h}{\partial x^3} - \frac{\partial}{\partial x}\left\{\left[\frac{\mathrm{d}}{\mathrm{d}h}\left(\frac{p_{\mathrm{dp}}}{\mathrm{We}}\right)\right]^{(-)}\frac{\Delta h}{2}\right\}$$
$$- \frac{2}{\mathrm{Re}}\frac{\partial^2 \Delta w}{\partial x^2} - \frac{2}{\mathrm{Re}}\frac{\partial \ln h^{(-)}}{\partial x}\frac{\partial \Delta w}{\partial x} - \frac{2}{\mathrm{Re}}\frac{\partial w^{(-)}}{\partial x}\frac{\partial}{\partial x}\left[\frac{\Delta h}{h^{(-)}}\right] = R_w^{(-)}. \tag{B.6}$$

To solve numerically Eqs. (B.5) and (B.6) we use a regular grid for the space coordinate, x, defined as $x_k = -1 + k\Delta x$ ($k = 0, 1, 2, \ldots, n$), where n is the number of intervals with a length $\Delta x = 2/n$. The values of the functions in the nodes of the grid are denoted with the subscript k. For example, the central difference in space with precision $O(\Delta x^2)$ applied to Eq. (B.5) gives

$$-\frac{w_{k-1}^{(-)}}{4\Delta x}\Delta h_{k-1} - \frac{h_{k-1}^{(-)}}{4\Delta x}\Delta w_{k-1} + \frac{\Delta h_k}{\Delta t} + \frac{w_{k+1}^{(-)}}{4\Delta x}\Delta h_{k+1} + \frac{h_{k+1}^{(-)}}{4\Delta x}\Delta w_{k+1} = R_{h,k}^{(-)}, \tag{B.7}$$

where

$$R_{h,k}^{(-)} = \frac{h_{k-1}^{(-)}w_{k-1}^{(-)} - h_{k+1}^{(-)}w_{k+1}^{(-)}}{2\Delta x} \tag{B.8}$$

and $k = 1, 2, \ldots, n-1$.

The respective difference scheme with precision $O(\Delta x^2)$ applied to Eq. (B.6) is

$$\left[\frac{\ln h_{k+1}^{(-)} - \ln h_{k-1}^{(-)}}{2\mathrm{Re}\Delta x^2} - \frac{w_{k-1}^{(-)}}{4\Delta x} - \frac{2}{\mathrm{Re}\Delta x^2}\right]\Delta w_{k-1}$$
$$+ \left\{\frac{w_{k+1}^{(-)} - w_{k-1}^{(-)}}{2\mathrm{Re}\Delta x^2 h_{k-1}^{(-)}} + \frac{1}{4\Delta x}\left[\frac{\mathrm{d}}{\mathrm{d}h}\left(\frac{p_{\mathrm{dp}}}{\mathrm{We}}\right)\right]_{k-1}^{(-)}\right\}\Delta h_{k-1}$$
$$+ \left(\frac{1}{\Delta t} + \frac{4}{\mathrm{Re}\Delta x^2}\right)\Delta w_k - \frac{1}{2\mathrm{We}}D_k(\Delta h)$$
$$+ \left[\frac{w_{k+1}^{(-)}}{4\Delta x} - \frac{2}{\mathrm{Re}\Delta x^2} - \frac{\ln h_{k+1}^{(-)} - \ln h_{k-1}^{(-)}}{2\mathrm{Re}\Delta x^2}\right]\Delta w_{k+1}$$
$$+ \left\{\frac{1}{2We\Delta x^3} - \frac{1}{4\Delta x}\left[\frac{\mathrm{d}}{\mathrm{d}h}\left(\frac{p_{\mathrm{dp}}}{\mathrm{We}}\right)\right]_{k+1}^{(-)} - \frac{w_{k+1}^{(-)} - w_{k-1}^{(-)}}{2\mathrm{Re}\Delta x^2 h_{k+1}^{(-)}}\right\}\Delta h_{k+1} = R_{w,k}^{(-)}, \tag{B.9}$$

where

$$R_{w,k}^{(-)} = \frac{w_{k-1}^{(-)}w_{k-1}^{(-)} - w_{k+1}^{(-)}w_{k+1}^{(-)}}{4\Delta x} + \frac{1}{\mathrm{We}}D_k[h^{(-)}]$$
$$+ \frac{p_{\mathrm{dp},k+1}^{(-)} - p_{\mathrm{dp},k-1}^{(-)}}{2\mathrm{We}\Delta x} + \frac{4}{\mathrm{Re}}\frac{w_{k+1}^{(-)} - 2w_k^{(-)} + w_{k-1}^{(-)}}{\Delta x^2}$$
$$+ \frac{w_{k+1}^{(-)} - w_{k-1}^{(-)}}{\mathrm{Re}\Delta x^2}\left[\ln h_{k+1}^{(-)} - \ln h_{k-1}^{(-)}\right] \tag{B.10}$$

and D_k is the difference operator representing the third derivative with respect to the space coordinate x.

Because of the third derivative with respect to x, the difference operator, D_k, in the nodes $k = 2, 3, \ldots, n-2$ has different form than those written for the nodes 1 and $n-1$. For $k = 2, 3, \ldots, n-2$ we use the following central difference expression for D_k [58],

$$D_k(f) = \frac{f_{k+2} - 2f_{k+1} + 2f_{k-1} - f_{k-2}}{2\Delta x^3}, \tag{B.11}$$

D_1 is defined by the relationship [58]

$$D_1(f) = -\frac{f_4 - 6f_3 + 12f_2 - 10f_1 + 3f_0}{2\Delta x^3}, \tag{B.12}$$

and D_{n-1} is calculated using the values of the function in the nodes $n-4$, $n-3$, $n-2$, $n-1$, and n through equation [58]

$$D_{n-1}(f) = \frac{3f_n - 10f_{n-1} + 12f_{n-2} - 6f_{n-3} + f_{n-4}}{2\Delta x^3}. \tag{B.13}$$

The matrix of the obtained linear system of equations, Eqs. (B.7) and (B.9), completed with the boundary conditions, Eqs. (3.5) and (3.6), written in terms of the unknown vector (Δh_0, Δw_0, Δh_1, Δw_1, Δh_2, Δw_2, …, Δh_{n-1}, Δw_{n-1}, Δh_n, Δw_n), contains 5 upper and 7 lower diagonals. The numerical solution of this system is performed efficiently using the Thomas algorithm [59]. The described numerical scheme is stable, of the second order of time, and is therefore, applicable for $\Delta t \approx \Delta x$.

References

[1] J. Sjoblom (Ed.), Emulsions and Emulsion Stability, second ed., CRC Taylor and Francis, Boca Raton, 2006.
[2] D. Exerowa, P.M. Kruglyakov, Foam and Foam Films: Theory, Experiment, Application, Elsevier Science, Amsterdam, 1998.
[3] I.B. Ivanov, K.D. Danov, P.A. Kralchevsky, Colloids Surf. A 152 (1999) 161–182.
[4] I.B. Ivanov, P.A. Kralchevsky, Colloids Surf. A 128 (1997) 155–175.
[5] I.B. Ivanov (Ed.), Thin Liquid Films, Marcel Dekker, New York, 1988.
[6] B.V. Derjaguin, N.V. Churaev, V.M. Muller, Surface Forces, Plenum Press, New York, 1987.
[7] K.S. Birdi (Ed.), Handbook of Surface and Colloid Chemistry, third ed., CRC Taylor and Francis, Boca Raton, 2008.
[8] J. Blawzdziewicz, E. Wajnryb, M. Loewenberg, J. Fluid Mech. 395 (1999) 29–59.
[9] A.K. Chesters, I.B. Bazhlekov, J. Colloid Interface Sci. 230 (2000) 229–243.
[10] J. Blawzdziewicz, V. Cristini, M. Loewenberg, J. Colloid Interface Sci. 211 (1999) 355–366.
[11] M.D. Ida, M.J. Miskis, SIAM J. Appl. Math. 58 (1998) 456–473.
[12] M.D. Ida, M.J. Miskis, SIAM J. Appl. Math. 58 (1998) 474–500.
[13] I.B. Ivanov, Pure Appl. Chem. 52 (1980) 1241–1262.
[14] A.K. Malhotra, D.T. Wasan, AIChE J. 33 (1987) 1533–1541.
[15] D.E. Tambe, M.M. Sharma, J. Colloid Interface Sci. 147 (1991) 135–151.
[16] D.S. Valkovska, K.D. Danov, J. Colloid Interface Sci. 241 (2001) 400–412.
[17] P. de Roussel, D.V. Khakhar, J.M. Ottino, Chem. Eng. Sci. 56 (2001) 5511–5529.
[18] S.D. Stoyanov, N.D. Denkov, Langmuir 17 (2001) 1150–1156.
[19] D.S. Valkovska, K.D. Danov, I.B. Ivanov, Adv. Colloid Interface Sci. 96 (2002) 101–129.
[20] M.B. Williams, S.H. Davis, J. Colloid Interface Sci. 90 (1982) 220–228.
[21] M. Prévost, D. Gallez, J. Chem. Phys. 84 (1986) 4043–4048.
[22] T. Erneux, S. Davis, Phys. Fluids A 5 (1993) 1117–1122.
[23] A. de Wit, D. Gallez, C.I. Christov, Phys. Fluids 6 (1994) 3256–3266.
[24] D. Vaynblat, J.R. Lister, T.P. Witelski, Phys. Fluids 13 (2001) 1130–1140.
[25] J.P. Burelbach, S.G. Bankoff, S.H. Davis, J. Fluid Mech. 195 (1988) 463–494.
[26] D. Hatziavramidis, J. Multiphase Flow 18 (1992) 517–530.
[27] K.D. Danov, N. Alleborn, H. Raszillier, F. Durst, Phys. Fluids 10 (1998) 131–143.
[28] K.D. Danov, V.N. Paunov, N. Alleborn, H. Raszillier, F. Durst, Chem. Eng. Sci. 53 (1998) 2809–2822.
[29] K.D. Danov, V.N. Paunov, S.D. Stoyanov, N. Alleborn, H. Raszillier, F. Durst, Chem. Eng. Sci. 53 (1998) 2823–2837.

[30] V.N. Paunov, K.D. Danov, N. Alleborn, H. Raszillier, F. Durst, Chem. Eng. Sci. 53 (1998) 2839–2857.
[31] S. Tabacova, L. Carotenuto, Microgravity Q 4 (1994) 55–61.
[32] A. Graciaa, G. Morel, P. Saulner, J. Lachaise, R.S. Schechter, J. Colloid Interface Sci. 172 (1995) 131–136.
[33] K.G. Marinova, R.G. Alargova, N.D. Denkov, O.D. Velev, D.N. Petsev, I.B. Ivanov, R.P. Borwankar, Langmuir 12 (1996) 2045–2051.
[34] V.N. Paunov, S.I. Sandler, E.W. Kaler, Langmuir 17 (2001) 4126–4128.
[35] L. Wang, R.-H. Yoon, Langmuir 20 (2004) 11457–11464.
[36] J.K. Angarska, B.S. Dimitrova, K.D. Danov, P.A. Kralchevsky, K.P. Ananthapadmanabhan, A. Lips, Langmuir 20 (2004) 1799–1806.
[37] L. Wang, R.-H. Yoon, Colloids Surf. A 263 (2005) 267–274.
[38] L. Wang, R.-H. Yoon, Colloids Surf. A 282–283 (2006) 84–91.
[39] M. Bosröm, D.R.M. Williams, B.W. Ninham, Phys. Rev. Lett. 87 (2001) 168103.
[40] J.N. Israelachvili, H. Wennerström, J. Phys. Chem. 96 (1992) 520–531.
[41] K.D. Danov, I.B. Ivanov, K.P. Ananthapadmanabhan, A. Lips, Adv. Colloid Interface Sci. 128–130 (2006) 185–215.
[42] L.G. Leal, Laminar Flow and Convective Transport Processes: Scaling Principles and Asymptotic Analysis, Butterworth-Heinemann, Stoneham, MA, 1992.
[43] M. Boström, W. Kunz, B.W. Ninham, Langmuir 21 (2005) 2619–2623.
[44] N.C. Christov, K.D. Danov, P.A. Kralchevsky, K.P. Ananthapadmanabhan, A. Lips, Langmuir 22 (2006) 7528–7542.
[45] J.T. Petkov, N.D. Denkov, K.D. Danov, O.D. Velev, R. Aust, F. Durst, J. Colloid Interface Sci. 172 (1995) 147–154.
[46] J.T. Petkov, K.D. Danov, N.D. Denkov, R. Aust, F. Durst, Langmuir 12 (11) (1996) 2650–2653.
[47] J.N. Israelachvili, Intermolecular and Surface Forces, Academic Press, London, 1992.
[48] B.U. Felderhof, J. Chem. Phys. 48 (1968) 1178–1185.
[49] B.U. Felderhof, J. Chem. Phys. 49 (1968) 44–51.
[50] S. Sche, H.M. Fijnaut, Surf. Sci. 76 (1978) 186–202.
[51] A.A. Mohamed, E.F. Elshehawey, M.F. El-Sayed, J. Colloid Interface Sci. 169 (1995) 65–78.
[52] L. Popova, G. Gromyko, S. Tabakova, Diff. Equat. 39 (2003) 1037–1043.
[53] D.S. Valkovska, K.D. Danov, I.B. Ivanov, Colloids Surf. A 156 (1999) 547–566.
[54] S.I. Karakashev, E.D. Manev, R. Tsekov, A.V. Nguyen, J. Colloid Interface Sci. 318 (2008) 358–364.
[55] D.A. Edwards, H. Brenner, D.T. Wasan, Interfacial Transport Processes and Rheology, Butterworth-Heinemann, Boston, 1991.
[56] C.A.J. Fletcher, Computational Techniques for Fluid Dynamics. 1. Fundamental and General Techniques, Springer-Verlag, New York, 1991.
[57] C.A.J. Fletcher, Computational Techniques for Fluid Dynamics. 2. Specific Techniques for Different Flow Categories, Springer-Verlag, New York, 1991.
[58] M. Abramowitz, I.A. Stegun, Handbook of Mathematical Functions, National Bureau of Standards, Washington, DC, 1984.
[59] W.H. Press, B.P. Flannery, S.A. Teukolsky, W.T. Vetterling, Numerical Recipes in FORTRAN: The Art of Scientific Computing, Cambridge Univ. Press, New York, 1992.